MOX-Report No. 10/2024

Personalized Computational Electro-mechanics Simulations to Optimize Cardiac Resynchronization Therapy

Capuano E.; Regazzoni F.; Maines M.; Fornara S.; Locatelli V.; Catanzariti D.; Stella S.; Nobile F.; Del Greco M.; Vergara C.

Personalized Computational Electro-mechanics Simulations to Optimize Cardiac Resynchronization Therapy

Emilia Capuano[1], Francesco Regazzoni[1], Massimiliano Maines[2], Silvia Fornara[3], Vanessa Locatelli[3], Domenico Catanzariti[2], Simone Stella[1], Fabio Nobile[4], Maurizio Del Greco[2], and Christian Vergara[3]

[1] *MOX, Dipartimento di Matematica, Politecnico di Milano, Milan, Italy*
[2] *Divisione di Cardiologia, Ospedale S. Maria del Carmine, Rovereto, Trento, Italy*
[3] *LABS, Dipartimento di Chimica, Materiali e Ingegneria Chimica "Giulio Natta", Politecnico di Milano, Milan, Italy*
[4] *EPFL, École Polytechnique Fédérale de Lausanne, Lausanne, Switzerland*

January 25, 2024

Abstract

In this study, we present a computational framework designed to evaluate virtual scenarios of Cardiac Resynchronization Therapy (CRT) and compare their effectiveness based on relevant clinical biomarkers. Our approach involves electro-mechanical numerical simulations calibrated, for patients with left bundle branch block, using data from Electro-Anatomical Mapping System (EAMS) measures, as well as ventricular pressures and volumes, both obtained pre-implantation. We validate the calibration by using EAMS data coming from right pacing conditions. Three patients with fibrosis and three without are considered to explore various conditions. Our virtual scenarios consist of personalized numerical experiments, incorporating different positions of the left electrode along reconstructed epicardial veins; different locations of the right electrode; different ventriculo-ventricular delays. The aim is to offer a comprehensive tool capable of optimizing CRT efficiency for individual patients, by providing preliminary answers on optimal electrode placement and delay.

1 Introduction

Cardiac Resynchronization Therapy (CRT) is a clinical treatment employed by cardiologists to treat heart failure patients affected by dyssynchronous ventricular contraction [1], due e.g to Left Bundle Branch Block (LBBB), an electrical conduction defect causing a late activation of the left ventricle (LV), and resulting in a lowered ejection fraction. The aim of CRT is to restore a coordinated ventricular motion, therefore improving systolic function and cardiac output [2, 3].

The functioning of CRT relies on an implantable device called *bi-ventricular pacemaker* that provides electrical stimuli to the heart chambers, through the insertion of electrodes, in order to restore the synchronism and a physiological contraction of the cardiac muscle.

Usually, CRT is performed by locating one electrode in the epicardial veins of the left ventricle and another one in the right ventricle at the level of the apex. Often, the two stimuli are characterized by a delay in order to improve CRT performance. Clinicians, at the moment of the procedure, need to select suitable electrodes locations and an effective value of the stimuli delay. There is no global agreement on the optimal procedure settings ensuring a success of the therapy and long-term benefit for the patients [4, 5]. Indeed, 30% of patients do not respond to CRT, as several clinical trials show, like MIRACLE [6]. For such reasons CRT still needs to be improved.

In this context, mathematical and computational cardiac models may support clinicians by enabling the virtual reproduction of the heart function under different working conditions, avoiding to resort to invasive and expensive procedures. Indeed, mathematical models describing the physics of the heart, both in physiological and pathological conditions, are becoming a powerful tool to support therapeutic planning for several cardiac disorders, i.e. arrhythmias, cadiomyopathies, myocardial infarction, heart failure [7, 8], and, as in the present case, LBBB and ventricular dyssynchrony [9, 10].

Cardiac models need in general to account for electrical propagation, mechanical contraction, and haemodynamics [11]. In view of CRT simulation and optimization, several computational studies have been performed

by different research groups (see the review [12] and Table 1). Some of them focused only on electrophysiology, guaranteeing high efficiency and exploiting ECG patients' acquisition, however neglecting any indication about the mechanical restoring; other studies relied on electromechanics (EM) models, possibly calibrated by means of electrical (mapping or ECG) and pressure-volume measures; in some cases patient's fibrosis has been accounted for.

Work	Real human LV	Fibrosis	EM	EP Calibration	MEC Calibration	Opt CRT
Kerckhoffs et al., 2003 [13]	×	×	✓	×	×	×
Kerckhoffs et al., 2009 [9]	✓[†]	×	✓	×	×	×
Sermesant et al., 2011 [14]	✓	✓	✓	✓	✓	×
Hyde et al., 2015 [15]	✓	×	×	×	×	×
Kayvanpour et al., 2015 [16]	✓	×	×	✓[*]	×	×
Crozier et al., 2016 [17]	✓	×	✓	×	✓	×
Costa et al., 2020 [18]	✓	✓	×	×	×	×
Reumann et al., 2007 [19]	✓	×	×	×	×	✓
Villongco et al., 2016 [20]	✓	✓	×	✓[*]	×	✓
Pluijmert et al., 2016 [21]	×	×	✓	×	×	✓
Lee et al., 2017 [5]	✓	✓	✓	×	✓	✓
Isotani et al., 2020 [22]	✓	✓	✓	×	✓	✓
Fan et al., 2022 [23]	×	✓	✓	×	✓	✓

Table 1: State of the art of some representative computational studies for simulating CRT. In the bottom part we highlighted those works that included some preliminary investigations about CRT optimization
[†] canine LV have been used
[*] calibration has been performed by means of ECG measures; otherwise, anatomical electrical mapping has been used

More recently, some work performed a virtual CRT optimization by varying the location of the electrodes and the stimuli delay. However, in all the cases the positioning of electrodes has not taken into account anatomical constraints such as coronary sinus and left ventricle epicardial veins. Moreover, only the acute scenario, i.e. what happens just after the device implantation, has been analyzed.

In this work, a patient-specific EM computational model [24] is employed to study different CRT scenarios in acute conditions by virtually moving the left electrode along the patient-specific coronary sinus and epicardial veins, as happens in the clinical setting. Moreover, we consider different right electrode locations and stimulation delays. For each of the analyzed patients we calibrated the model electrical properties by using electro-anatomical mappings, as proposed in [25, 26], and mechanical properties by using volume and pressure measures. At the best of our knowledge, this is the first computationally study that exploits patient-specific anatomically compatible locations of the left electrode in CRT studies. Moreover, for the first time, we used a calibrated EM model for CRT optimization and we explore different right electrode positions.

Six real cases of patients implanted with a CRT device are presented, all affected by LBBB and all treated at the S. Maria del Carmine Hospital in Rovereto (TN), Italy, by using the Latest Electrically Activated Segment (LEAS) in the epicardial veins to locate the left electrode. Pre-operative electrical and mechanical clinical measurements have been employed to calibrate the Eikonal-Reaction-Mechanics (ERM) model [27, 24] on each patient, whereas electrical measures obtained by an intermediate right pacing, carried out during the CRT implantation procedure,

have been used to validate our model.

The idea is to use the calibrated ERM model to provide useful information about the optimal CRT scenario for the patient, by comparing activation and contraction of different virtual configurations just after the implantation of the device. This is justified by assuming that the haemodynamic and electrical properties characterizing the patient do not change immediately after the beginning of CRT stimulation. The beneficial effects of every CRT scenario are evaluated and compared using suitable mechanical biomarkers, that are used in clinical practice to evaluate acute outcomes of the therapy [14, 28]. Such quantities are able to provide information about the restoring of the heart function, such as the Ejection Fraction (EF) and the maximum rate of pressure change, that can be easily computed as post-processing of the numerical ERM results.

2 Materials and methods

2.1 Overview of the work

The overall flowchart of the method we developed to perform virtual CRT scenarios and compare their outcomes is mainly composed by three major steps:

- Pre-processing of the data in order to obtain the computational meshes and the activation times provided by electro-anatomical mapping procedures;

- Calibration of the Eikonal-Reaction-Mechanics model in terms of both electrical and mechanical parameters, in sinus rhythm (pre-operative) conditions;

- Simulation of CRT virtual scenarios by varying left and right electrodes positions and delay.

In Figure 1 we report the complete flowchart of the steps of our strategy, that will be detailed in the following paragraphs.

2.2 Clinical data

We have at disposal six patients (referred in what follows as P2, P3, P4, P6, P8, P11, in accordance with previous numbering) who underwent CRT at Santa Maria del Carmine Hospital, Rovereto (TN), Italy. All the patients suffered from ventricle dyssynchrony caused by LBBB. Patients P6, P8, P11 presented fibrotic regions.

For all the patients we had at disposal different sets of data referring to the pre-operative scenario that were processed as follows:

- MRI images used for the segmentation and reconstruction of the left ventricle geometry. These allowed us to build the computational meshes for the numerical simulations (see [25] for further details);

- Bullseye diagram highlighting the fibrotic regions distribution in terms of the 17-segment division of the LV myocardium. See Figure 2;

- Electrical activation times obtained during sinus rhythm (pre-operative scenario) with the contact *EnSite Precision^{TM}* Electro-Anatomical Mapping System (EAMS) [29], whose utility was threefold. First, measurements of activation times in the septal region, when available, were used as input to the electrical propagation model during the electrical calibration (pre-operative conditions). Secondly, measurements at the coronary sinus were used to calibrate electrical conductivities [26]. Finally, the spatial distribution of acquisition points along the lateral LV epicardium was used to identify the epicardial veins geometry (See Figure 2 and [25] for further details);

- Electrical activation times obtained during right pacing (only right electrode active) with EAMS. These data are acquired by cardiologists as a preliminary analysis before CRT implantation and will be used in this study to validate the electrical calibration obtained using pre-operative data;

- Measures of the End Systolic and Diastolic Volumes (ESV and EDV) obtained by MRI (with corresponding stroke volume (SV) and ejection fraction (EF)), and of diastolic and systolic pressure values (denoted as P_D and P_S) measured at the arm, together with the heart rate (HR). See Table 2.

Finally, we notice that we have at disposal also CT images for another case (P12), which are used for a validation of the epicardial veins reconstruction. Starting from these images, we reconstruct the coronary veins applying in the `vmtk` software the *vesselness* filter provided in [30] as a pre-processing step for a better visualization of the lumen of the vessel. We then performed a level set segmentation after a colliding fronts initialization [31].
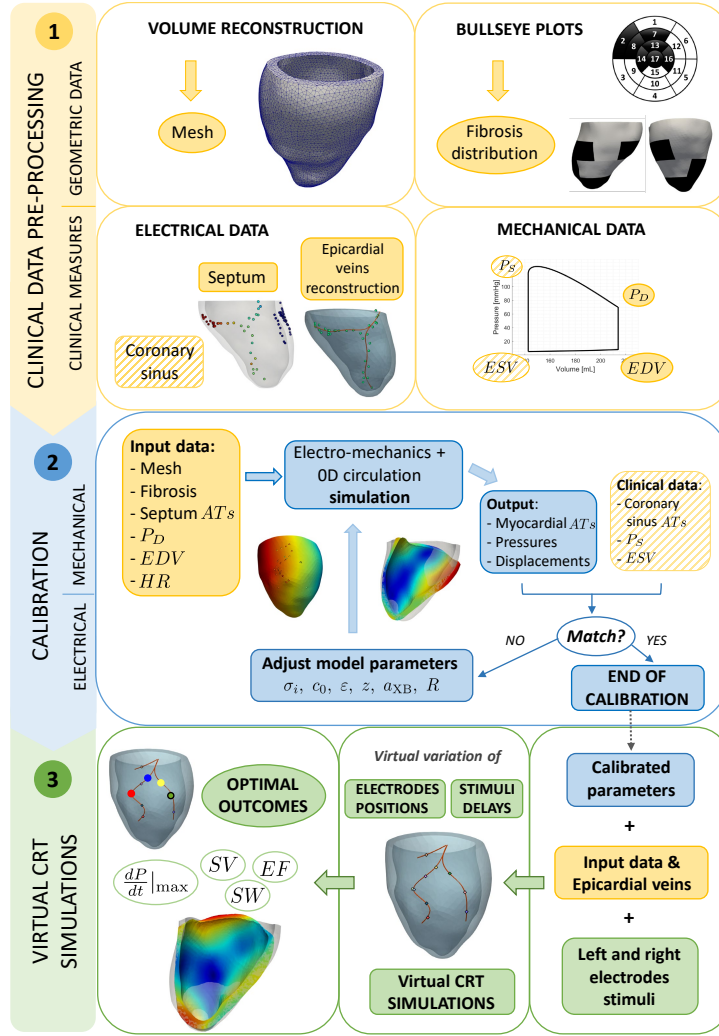
Figure 1: Pipeline of the overall method. Top, yellow sector: Pre-processing procedures to obtain the input data; Middle, blue sector: Electrical and mechanical calibrations to obtain the personalized parameters; Bottom, green sector: Virtual CRT simulations. AT stands for Activation Times.

	ESV [ml]	EDV [ml]	SV [ml]	EF [%]	P_D [mmHg]	P_S [mmHg]	HR [bpm]
P2	425	501	76	15.2	60	110	85
P3	238	350	112	32.0	75	140	75
P4	226	300	73	24.5	80	120	62
P6	236	318	82	25.8	70	110	76
P8	143	214	71	33.2	70	130	68
P11	173	231	58	25.1	80	110	110

Table 2: Clinical data used for the mechanical calibration, together with the heart rate.

2.3 Mathematical Model

For the computational model we used the *Eikonal-Reaction-Mechanics* (ERM) model proposed in [24], so that we refer the interested reader there for details. Here, it is enough to report the coupled models and the relevant parameters for the calibration:

1. An offline Eikonal-Diffusion model [32] to determine activation times ψ in electrophysiology, see in particular [24]. This is characterized by parameter c_0 that tunes the velocity of the depolarization wave along the fiber direction for a planar wavefront, by the dimensionless parameter ε that regulated the impact of the

4
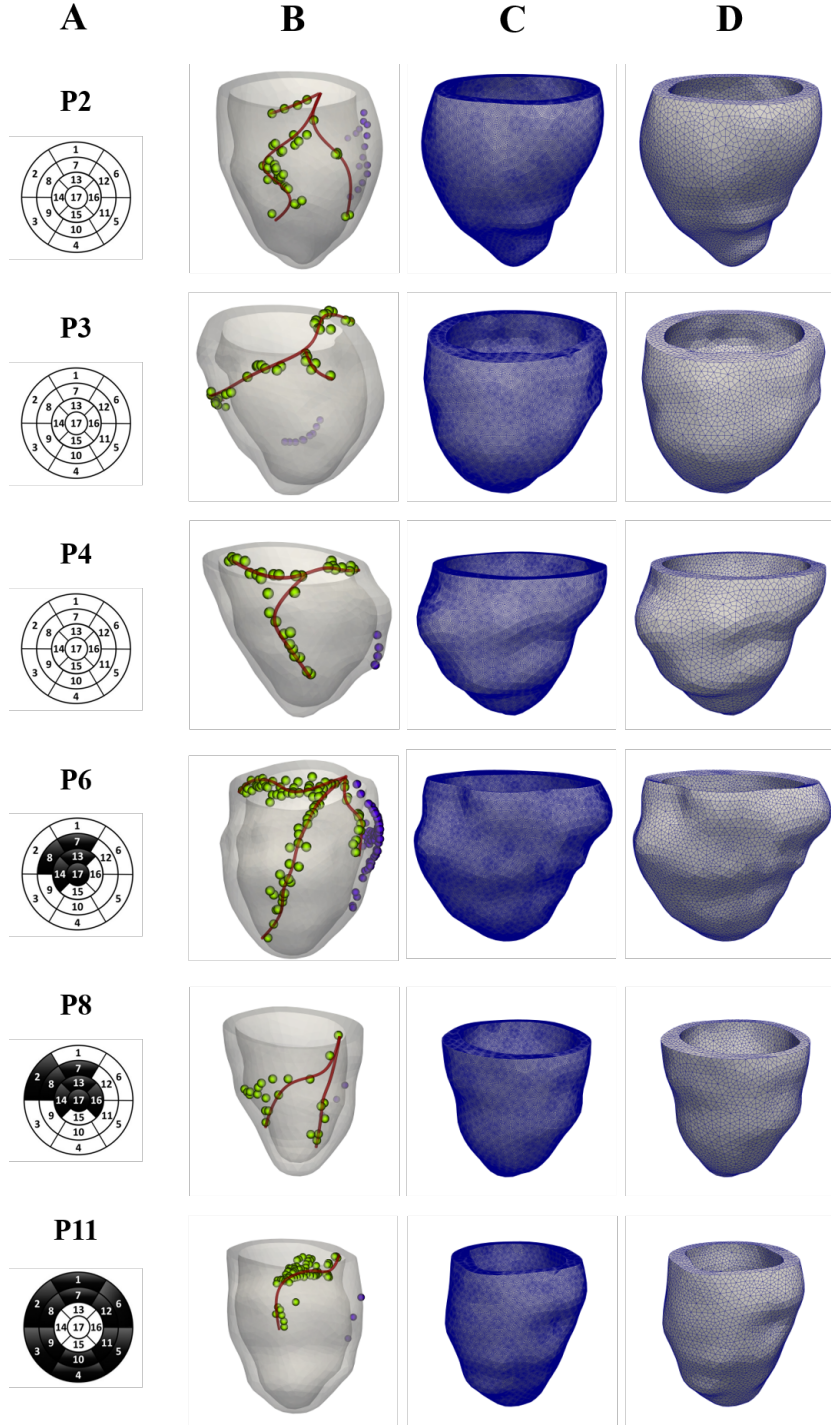
Figure 2: From the left: A) 17-level segments bullseye plots of the ischemic regions; B) Patient's reconstructed LV and epicardial veins geometries, together with points of EAMS measures. In green the measure points used for the veins' reconstruction; C) Fine mesh for electrophysiology simulations; D) Coarse mesh for mechanics simulations.

wavefront curvature on its propagation velocity, and by the conductivity tensor normalized with respect to the surface-to-volume ratio χ and the transmembrane capacitance C_m (see [24]):

$$\widehat{\mathbf{D}} = z\widehat{\sigma}_s \mathbf{1} + z(\widehat{\sigma}_f - \widehat{\sigma}_s)\boldsymbol{f} \otimes \boldsymbol{f} + z(\widehat{\sigma}_n - \widehat{\sigma}_s)\boldsymbol{n} \otimes \boldsymbol{n}. \tag{1}$$

Vectors $\boldsymbol{f}$, $\boldsymbol{s}$ and $\boldsymbol{n}$ are the fibers, sheets and normal directions, $\{\widehat{\sigma}_i\}_{i \in \{f,s,n\}}$ are the respective conductivities and $z \in [0, 1]$ indicates the degree of fibrosis (with $z = 1$ denoting an healthy tissue);

2. The solution ψ obtained at step (i) is in turn used to shift the calcium transient precomputed by solving an offline Reaction problem [27] for the intracellular calcium concentration $[\text{Ca}^{2+}]_i$, namely a simplified version of the monodomain equation, coupled to the *ToR-ORd* ionic model [33];

3. The temporal loop where at each time-step we have the coupling among:

   (a) The mechanical activation (MA) provided by the *RDQ20-MF* model [34], characterized by *cross-bridge stiffness* a_{XB}, which quantifies the myocardial tissue contractility. This allows to compute the active tension T_a;

   (b) The active-passive mechanics (APM); in particular we used the *Usyk constitutive law* [35] for the passive mechanics and the active stress obtained by assuming that T_a acts only in the fibers direction $\boldsymbol{f}$ [36];

   (c) A two-element Windkessel (W) model for the circulatory system during the ejection phase [37, 38], characterized by the resistance R and the compliance C, or a linear ramp for the pressure during the filling phase.

Specifically, MA provides the active tension for APM, whereas the latter allows us to prescribe the mechanical deformation to the former. APM and W are coupled during the ejection phase, through the exchange of LV pressure and volume, whereas during the filling the pressure data of the prescribed ramp are assigned to APM. On the other hand, isovolumetric phases have been managed by interpreting the 0D pressures as Lagrange multipliers to enforce the volume conservation constraint. To account for the pericardium APM model was equipped by Robin-like boundary conditions [39].

Notice that the electrophysiology problem (steps i and ii) is based on computing the activation times $\psi(\boldsymbol{x})$ with an Eikonal model and then to localize in the Reaction problem an applied current for each point $\boldsymbol{x}$ in a temporal neighborhood of $\psi(\boldsymbol{x})$. This allowed us to surrogate the diffusion process [24].

Since electrical propagation and mechanical contraction is highly influenced by cardiac fibers' direction and standard imaging techniques do not provide geometric information, we used here the Laplace-Dirichlet rule-based algorithm described in [40, 41], see also [25] for further details.

We highlight also that the previous model is based on the simplifying assumption of neglecting the *mechano-electrical feedbacks*, allowing to solve electrophysiology (step i and ii) outside of the temporal loop. The solution of the Reaction model (step ii) is obtained off-line for each heartbeat duration and evaluated in each mesh point.

The choice of using a 0D model for blood fluid-dynamics is justified by the major interest of the present work in the electrical and mechanical contraction of the cardiac muscle, rather than blood dynamics in the chamber.

In Figure 3 we report a comprehensive picture of the computational model.
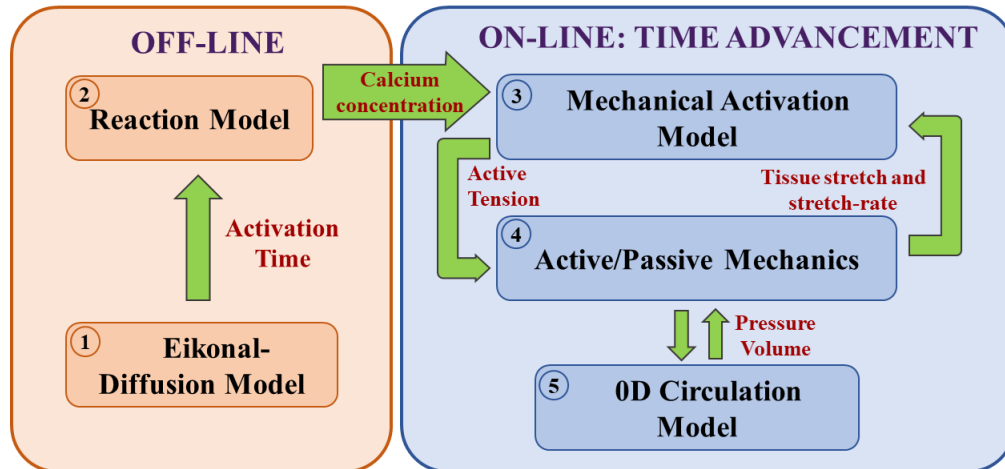
Figure 3: Structure of the Eikonal-Reaction-Mechanics model, highlighting the couplings among the different cores.

2.4 Numerical Approximation

All computational methods for the numerical approximation of the ERM mathematical model are implemented in the high-performance C++ library life$^{\text{x}}$, developed at MOX, Dipartimento di Matematica, with the collaboration

of LaBS, Dipartimento di Chimica, Materiali e Ingegneria Chimica (both at Politecnico di Milano) [1] [42, 43].

For the numerical solution of time-dependent problem (iii) in Section 2.3, we consider a segregated method, based on a loosely-coupled strategy for mechanics couplings with both MA and 0D model [24]. We discretize all the evolutionary subproblems by means of the BDF1 scheme using a time-step $\Delta t = 1 \times 10^{-4}$ s. MA problem, which is instead approximated by the Forward Euler method, requires a finer time step for numerical stability purposes. Hence, it is advanced resorting to an inner iteration loop with $\Delta t = 2.5 \times 10^{-5}$ s (see [24]).

Each subproblem is discretized in space using the Finite Element Method (FEM) of order 1 on hexahedral meshes (Q1). Two nested meshes are genereted: a coarser mesh for mechanics ($h \simeq 3.5$ mm) and a finer one for electrophysiology ($h \simeq 0.8$ mm) obtained by recursively splitting each element of the coarser one. See Figure 2.

2.5 Calibration

To calibrate the model in pre-operative conditions, we proceed in two steps, considering first the electrophysiology and then the mechanics, due to the absence of feedback from the latter to the former. The values of all the other non-calibrated parameters used in the numerical experiments are reported in Table 3, together with the default initial values from which our calibration procedure started.

	SL_0 [µm]	k_d [µM]	α_{k_d} [µM/µm]	γ [−]
MECHANICAL ACTIVATION	2.2	0.4	−0.2083	30
	k_{off} [s^{-1}]	k_{basic} [s^{-1}]	$\mu^0_{f_\mathcal{P}}$ [s^{-1}]	$\mu^1_{f_\mathcal{P}}$ [s^{-1}]
	40	8	32.255	0.768
PERICARDIUM	$K^{\text{epi}}_\perp$ [Pa m^{-1}]	$K^{\text{epi}}_\parallel$ [Pa m^{-1}]	$C^{\text{epi}}_\perp$ [Pa s m^{-1}]	$C^{\text{epi}}_\parallel$ [Pa s m^{-1}]
	$2 \cdot 10^5$	$2 \cdot 10^4$	$2 \cdot 10^4$	$2 \cdot 10^3$
WINDKESSEL	$\bar{p}^{0D}_{\text{MVO}}$ [mmHg]	$\bar{p}^{0D}_{\text{ED}}$ [mmHg]	C [m^3 Pa^{-1}]	
	5	10	$4.5 \cdot 10^{-9}$	

Table 3: Non-calibrated parameters used in the numerical simulations: Mechanical Activation parameters taken from [34], Pericardium and Windkessel parameters taken from [24].

2.5.1 Electrical calibration

We prescribe as input to the Eikonal-Diffusion model the activation times measured at the septum. When these are not available (i.e. for P8 and P11), three equispaced points are selected at the septum, to surrogate the action of the Purkinje network. Then, we calibrate the Eikonal-Diffusion model parameters, following the criterion of minimizing the discrepancy between the clinically measured activation times t_i^{clin}, representing the pre-operative scenario, on the epicardial veins and their computational counterparts t_i^{comp} (calibration error):

$$e[\%] = \frac{1}{NT_{\max}} \sum_{i=1}^{N} |t_i^{\text{clin}} - t_i^{\text{comp}}| \cdot 100, \tag{2}$$

where N is the number of activation times clinically recorded and $T_{\max}$ is the maximum activation time recorded. Due to the computational challenges linked to automatic optimization procedures with an underlying differential model, we rely on a manual procedure. Specifically, starting from baseline values [24], we iteratively tune the parameters (the parameter c_0 is employed to control the action potential speed propagation, while the dimensionless parameter ε controls the wave curvature effect) until the relative error e is lower than a prescribed threshold of 10%. In patients with scarred tissue, we assign $z = 1$ in (1) in the healthy region, while, in the fibrotic region, we calibrate the value $z < 1$ by following the procedure described above, that is by minimizing (2). The rationale followed here is that a lower value of z slows down in a more pronounced way the action potential propagation in the considered region.

2.5.2 Mechanical calibration

Once the electrical calibration is successfully concluded, we proceed with the calibration of the mechanical and haemodynamic parameters. Some parameters of the model are readily available as patients' measures, namely the

---

[1] https://lifex.gitlab.io/lifex

HR, the EDV and the aortic valve opening pressure, which we surrogate with the clinically measured diastolic pressure P_D. We remark that the HR is not only used in the APM model to define the heartbeat period, but it is also employed to compute the calcium transient within the ToR-ORd ionic model, which has been calibrated based on human data [33], and is capable to reproduce the frequency-calcium response of ventricular cardiomyocytes. The calcium transient is provided to the RDQ20-MF model, which in turn faithfully reproduces the calcium-force response [34]. In this manner, our ERM model captures the rate-dependent effects of the heartbeat mechanics.

Finally, we employ the two remaining clinical quantities available, namely ESV and P_S, to calibrate two parameters of the model that rule the cardiac contractility and the afterload. These parameters are the cross-bridge stiffness a_{XB} and the Windkessel resistance R, respectively. Due to the higher computational cost of the APM model compared to the Eikonal-Diffusion model, following an iterative procedure by running the full-order APM model for any change of model parameters would entail a significant computational cost. Hence, in order to speedup this step of the calibration pipeline, we rely on the cardiac emulator proposed in [44]. The emulator is a surrogate cardiac model, built through a data-driven approach from a few Pressure-Volume (PV) loops computed through the computational model. Once it is constructed, it allows predicting PV loops for new values of the parameters in less than one millisecond on a single-core laptop, with an approximation lower than 1%. The workflow is thus as follows:

1. Run a few cycles with an initial guess of R and for two different values of a_{XB};

2. Construct the cardiac emulator, by relying on the Python library `cardio-emulator`[2];

3. Find the optimal value of the parameters a_{XB} and R by fitting ESV and P_S with the cardiac emulator prediction (we notice that this step is computationally fast, thanks to the use of the lightweight emulator);

4. Run a 3D-0D simulation with the selected parameters, to check that the fit of clinical data is satisfactory.

2.6 CRT scenarios under investigation

To study the optimal CRT configurations in acute conditions, the idea of this paper is to virtually vary the activation conditions of the stimulation by assuming that the electrical and mechanical conditions just after the implantation are the same of the pre-operative case. Indeed, CRT induces significant effects on the cardiac muscle only some months after the implant [45].

In what follows, we refer to LEAS as the *Latest Electrically Activated Segment*, i.e. the point accessible through the reconstructed epicardial veins characterized by the highest computed activation time. LEAS is used by some cardiologists for the location of the left electrode [46]. Notice that in [26] we proved that computational methods are able to well predict LEAS position.

In this study, we investigate the effect on CRT outcomes induced by three virtual modifications of the implant (see Figure 4, bottom):

- The left lead position is virtually placed in the LEAS (simulating a common practice of cardiologists) and in other permitted positions along the reconstructed epicardial veins. In this case the right lead is by default located in the LV epicardium (representing the RV apical endocardium) below the interventricular septum and close to the apex [46];

- The right lead position is also virtually placed in different points along the ventricle septum, keeping the left electrode fixed at LEAS;

- The ventriculo-ventricular delay (VVD) is virtually changed to account for different plausible values used by clinicians, with the convention that positive values indicates that the right stimulation precedes the left one.

We notice that for patients P8 and P11 the fibrotic region spreads out in a wide region, so that a limited (null for P11) area of healthy tissue is covered by the reconstructed epicardial veins. Thus, for these cases the location of the left electrode may be in a fibrotic region, see Results and Discussion sections.

In this work, we decided to use the preload values (i.e. diastolic pressure and volume) resulting from pre-operative measures also in the CRT scenarios. It is known that atrio-ventricular delay induced by the electrode located in the right atrium could however lead to different preload configurations during CRT [47]. This aspect has been here neglected since we are not considering the right atrium pacing.

---

[2]https://github.com/FrancescoRegazzoni/cardioemulator
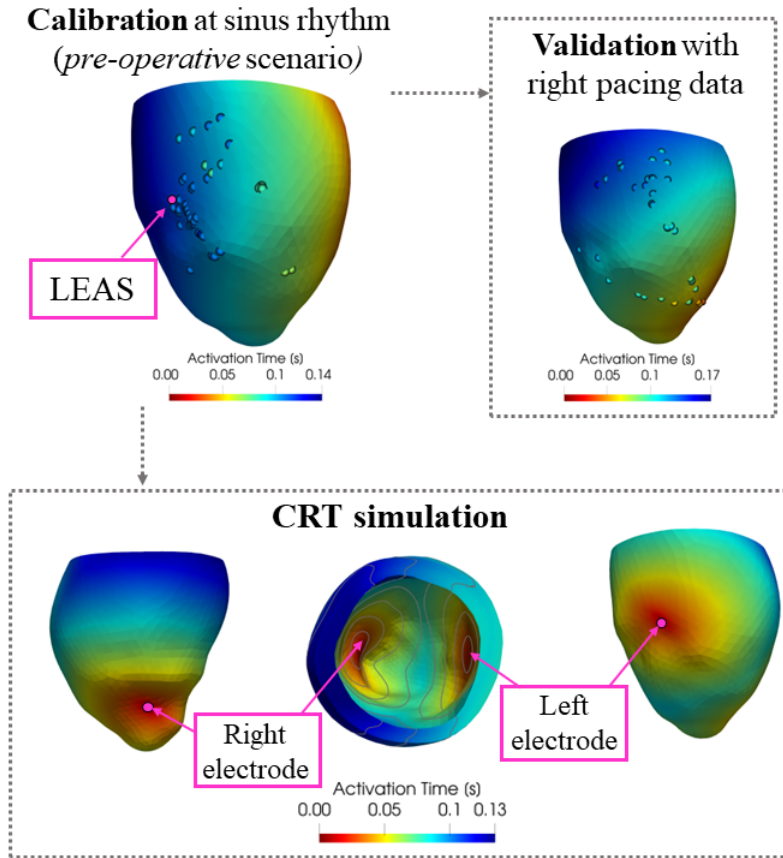
Figure 4: Computed activation times during calibration with corresponding data acquired at sinus rhythm (top left) and during validation with corresponding data acquired at right pacing (top right). Bottom: Example of computed activation times under CRT stimulation. Case P2.

3 Results

3.1 Validation of epicardial veins reconstruction

As highlighted in Section 2.2, the reconstruction of epicardial veins, useful for virtually changing the left electrode position, was obtained by means of the electrical activation times acquired by EAMS, as described in [25]. In order to show the validity of such strategy, we present here a comparison for P12 between this reconstruction and the standard one based on CT images at disposal, described in Section 2.2.

In Figure 5 we show the results of such comparison which highlight the suitability of the method proposed in [25] and used in this work to identify the epicardial veins.
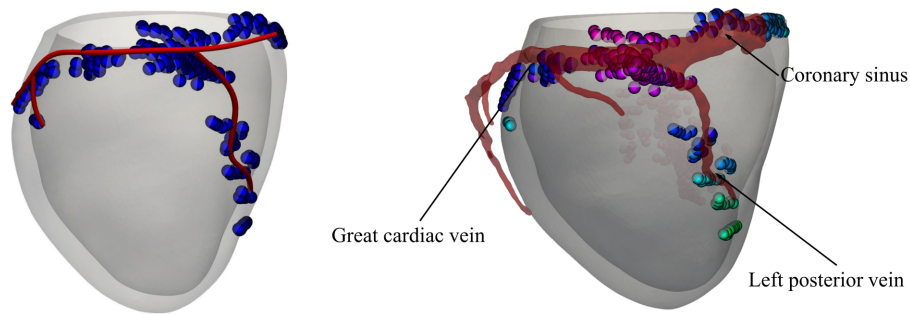
Figure 5: Validation of the reconstructed veins of patient P12 using EAMS measures (on the left) versus CT scan acquired image (in transparency on the right).

3.2 Calibration and validation

The results of the calibrated pre-operative simulations are presented in Figure 6, first and third columns. We notice that we have two classes of patients, namely the non-fibrotic ones (P2, P3, P4) and the fibrotic ones (P6, P8, P11).

In Table 4 we report the parameters values obtained from the calibration of the electrical, mechanical and 0D haemodynamics models, as well as the calibration errors obtained for the electrical function and computed using (2). It is worth noticing that they are all below the 10% threshold. In particular, calibration of patient P8 led to the highest error, probably due to the smaller number of available measures of activation times registered at the coronary sinus.

	P2	P3	P4	P6	P8	P11
ELECTRICAL						
$\widehat{\sigma}_f\ [10^{-4}\cdot\mathrm{m}^2\,\mathrm{s}^{-1}]$	2.29	1.99	1.37	1.91	1.91	1.57
$\widehat{\sigma}_s\ [10^{-4}\cdot\mathrm{m}^2\,\mathrm{s}^{-1}]$	1.05	0.91	0.62	0.87	0.87	0.72
$\widehat{\sigma}_n\ [10^{-4}\cdot\mathrm{m}^2\,\mathrm{s}^{-1}]$	0.34	0.29	0.20	0.28	0.28	0.23
$c_0\ [\mathrm{s}^{-\frac{1}{2}}]$	84.37	73.36	77.03	73.36	80.70	73.36
$\varepsilon\ [-]$	11.96	14.95	14.20	19.46	14.95	14.95
$z\ [-]$	1.0	1.0	1.0	0.7	0.7	0.9
Calibration error [%]	4.0	6.1	7.3	5.9	9.9	4.6
Validation error [%]	7.8	4.9	4.1	3.4	6.0	-
MECHANICAL						
$a_{\mathrm{XB}}\ [10^2\cdot\mathrm{MPa}]$	2.70	3.07	3.21	2.66	1.87	2.06
WINDKESSEL						
$R\ [10^7\cdot\mathrm{Pa\,s\,m}^{-3}]$	3.40	3.00	3.92	2.8	5.60	3.50

Table 4: Calibrated electrical, mechanical and Windkessel parameters, together with calibration and validation errors (except for P11 because of missing data of right pacing).

In order to assess the suitability of the calibration of the electrical parameters obtained by means of pre-operative activation times, we performed a validation by comparing the numerical results of the Eikonal problem against data not used in the calibration itself (cross validation). To this aim, we used the activation times acquired with EAMS during right pacing procedure we had at disposal (only right electrode at the apex is stimulating) and we performed numerical simulations in the right pacing scenario (see Figure 4, top).

In Table 4 we report the values of the relative errors obtained by this validation procedure (validation error), using a formula analogous to (2). We observe the excellent matching between the computed and the measured activation times in right pacing conditions. Since the measured data were not used in the calibration procedure, we can definitively state that our calibration has been successfully cross-validated.

The calibrated parameters are then used in turn for the simulations of the virtual CRT scenarios, whose analysis is presented in the next paragraphs.

In Figure 6 we report for all the patients the activation times and the mechanical displacements at a representative time instant for both the pre-operative and the LEAS-CRT scenarios. Notice that the activation times are in accordance with the fibrotic regions depicted in Figure 2. Moreover, the results on displacements provide an evidence that LEAS-CRT improves synchronism with respect to the pre-operative case.

3.3 Optimal left lead location

In Figure 7, left, we report our choices about the anatomically compatible locations inside the epicardial veins of the left electrode considered in our virtual CRT simulations. In the same figure, on the right we report and compare the corresponding PV loops. Notice that for all the patients the Stroke Volume (SV) (i. e. difference between diastolic and systolic volumes, $EDV - ESV$), and thus the ejection fraction $EF = SV/EDV$, increase for almost all virtual CRT scenarios with respect to the pre-operative case.

In Table 5 we report the specific values of SV and EF for the most representative virtual CRT scenarios.

From these results, we first notice that for the non-fibrotic cases LEAS is an effective choice in terms of improvements of the two biomarkers with respect to the pre-operative cases. Moreover, we notice that for P2 and P3 it is possible to obtain a further improvement by selecting a different left electrode location. Also for the fibrotic cases significant improvements of SV and EF were found for P6 and P11, with no further improvement by changing the left electrode location. Instead, for P8 LEAS reveals to be a non optimal choice, with VEIN1 location which is able

to provide a small improvement. Summarizing we have a maximum improvement with respect to the pre-operative case of SV in the percentage range $[7.3\%, 14.5\%]$ for the non-fibrotic cases and of $[4.2\%, 11.8\%]$ for the fibrotic cases; for EF we have a maximum improvement in the absolute range $[1.4, 3.1]$ (no significant differences between the two groups).

Patient	Location	$dP/dt|_{\max}$ [mmHg s^{-1}]	SV [ml]	EF [%]	SW [mmHg ml]
P2	*Pre-operative*	$2,252$	76	15.1	$6,300$
	LEAS	$+7.4\%$	$+11.8\%$	$+1.8$	$+19.4\%$
	VEIN 1	$+8.1\%$	$+14.5\%$	$+2.3$	$+23.5\%$
	VEIN 4	$+12.0\%$	$+11.8\%$	$+1.9$	$+20.1\%$
P3	*Pre-operative*	$3,119$	112	31.9	$11,600$
	LEAS	$+13.0\%$	$+8.0\%$	$+2.6$	$+14.8\%$
	VEIN 1	$+9.7\%$	$+9.8\%$	$+3.1$	$+16.5\%$
	VEIN 2	$+13.9\%$	$+8.0\%$	$+2.7$	$+17.3\%$
P4	*Pre-operative*	$2,278$	73	24.5	$6,800$
	LEAS	$+6.5\%$	$+7.3\%$	$+1.8$	$+10.8\%$
	VEIN 1	$+3.1\%$	$+6.3\%$	$+1.5$	$+10.0\%$
	VEIN 4	$+6.6\%$	$+1.9\%$	$+0.5$	$+3.7\%$
P6	*Pre-operative*	$2,186$	82	25.9	$7,000$
	LEAS	$+3.7\%$	$+11.8\%$	$+3.0$	$+16.9\%$
	VEIN 1	$+2.0\%$	$+10.8\%$	$+2.8$	$+15.4\%$
P8	*Pre-operative*	$2,731$	70	32.9	$6,700$
	LEAS	-7.5%	-1.4%	-0.3	-1.6%
	VEIN 1	$+2.0\%$	$+4.2\%$	$+1.4$	$+6.6\%$
P11	*Pre-operative*	$2,460$	58	25.0	$4,900$
	LEAS	$+0.7\%$	$+10.3\%$	$+2.6$	$+15.6\%$
	VEIN 4	$+1.5\%$	$+6.9\%$	$+1.9$	$+12.4\%$

Table 5: Biomarkers corresponding to virtual CRT configurations varying left lead position. See Figure 7 for the different locations of the left electrode. For CRT scenarios we indicate the percentage of variation of $dP/dt|_{\max}$, SV and SW with respect to the pre-operative case, whereas for EF we indicate the absolute changes. P2, P3, P4: non-fibrotic cases; P6, P8, P11: fibrotic cases.

In Table 5 other biomarkers are presented. Specifically, we computed the maximal LV pressure rise $dP/dt|_{\max}$ [48] occurring during systole. $dP/dt|_{\max}$ is used as an index of ventricular performance [49, 50] and thus elevated values of $dP/dt|_{\max}$ may be a sign, during the acute phase, of significant contractility and resynchronization [51]. Again, we notice that LEAS is an effective choice for the non-fibrotic cases, whereas for fibrotic case no significant improvements are noticed. Moreover, for P2 and P3 different left electrode locations provide a further improvement in terms of $dP/dt|_{\max}$. In any case, we notice that for all the CRT scenarios this index features larger values than the pre-operative case, being maximum improvements with respect to pre-operative case in the percentage range $[6.6\%, 13.9\%]$ for the non-fibrotic cases and $[1.5\%, 3.7\%]$ for the fibrotic cases. Another useful index reported in Table 5 is the Stroke Work (SW) defined as the work done by the ventricle to eject the blood and corresponding to the area within the PV loop. Analogously to the other biomarkers, LEAS is shown to be in general an effective choice and the value resulting from CRT simulations significantly increases with respect to pre-operative case in the ranges $[10.8\%, 23.5\%]$ for the non-fibrotic cases and $[6.6\%, 16.9\%]$ for the fibrotic cases.

3.4 Study of the ventriculo-ventricular delay

In Figure 8 we report the PV loops obtained by using LEAS for the left electrode and varying the ventriculo-ventricular delay VVD with the values $VVD = [-30, -15, 15, 30]$ ms, with the convention that positive values indicate that the right stimulus anticipates the left one. We observe that we obtain quite similar behaviors to the $VVD = 0$ scenario, in any case with an increased stroke volume with respect to the pre-operative one. Negative VVD, specifically $VVD = -30$ ms, seem to provide however slightly worst improvements.

These observations are confirmed by Table 6, where we report the same biomarkers of the previous analysis for the best positive and negative values of VVD. In particular, for the non-fibrotic cases we observe that positive values of VVD always allow to improve the four biomarkers with respect to the *synchronous* case $VVD = 0$, especially for

$dP/dt|_{\max}$. Instead, negative values of VVD, although improving the biomarkers with respect to the pre-operative case, do not seem to perform better than the synchronous case. As regards the fibrotic cases, we observe not significant improvements of the delayed cases with respect to the synchronous case.

Patient	Delay [ms]	$dP/dt\|_{\max}$ [mmHg s^{-1}]	SV [ml]	EF [%]	SW [mmHg ml]
P2	Pre-operative	2,252	76	15.1	6,300
	−15	+5.2%	+10.5%	+1.6	+17.0%
	0	+7.4%	+11.8%	+1.8	+19.0%
	30	+11.3%	+10.5%	+1.7	+18.0%
P3	Pre-operative	3,119	112	31.9	11,600
	−15	+7.0%	+7.1%	+2.3	+12.2%
	0	+13.0%	+8.0%	+2.6	+14.8%
	30	+24.9%	+8.9%	+2.8	+16.6%
P4	Pre-operative	2,278	73	24.5	6,800
	−15	+1.2%	+6.2%	+1.5	+9.8%
	0	+6.5%	+7.3%	+1.8	+10.8%
	15	+9.8%	+7.6%	+1.8	+10.9%
P6	Pre-operative	2,186	82	25.9	7,000
	−15	+2.4%	+11.5%	+3.0	+16.6%
	0	+3.7%	+11.8%	+3.0	+16.9%
	30	+6.7%	+9.7%	+2.5	+13.4%
P8	Pre-operative	2,731	70	32.9	6,700
	−15	−0.9%	+2.8%	+1.1	+6.9%
	0	+2.0%	4.2%	+1.4	+6.6%
	15	+3.0%	+4.2%	+1.5	+6.9%
P11	Pre-operative	2,460	58	25.0	4,900
	−15	+0.5%	+6.9%	+2.1	+12.4%
	0	+0.7%	+10.3%	+2.6	+15.6%
	15	−0.9%	+8.6%	+2.2	+13.2%

Table 6: Biomarkers corresponding to virtual CRT configurations varying ventriculo-ventricular delay (VVD) with the left electrode positioned at LEAS. Positive values of VVD means that the right stimulation occurs before the left one. For CRT scenarios we indicate the percentage of variation of $dP/dt|_{\max}$, SV and SW with respect to the pre-operative case, whereas for EF we indicate the absolute changes. P2, P3, P4: non-fibrotic cases; P6, P8, P11: fibrotic cases.

3.5 Study of the right electrode location

In this section, we report the results obtained by varying the position of the right electrode along the interventricular septum, while keeping the left one fixed at LEAS and without any VVD. In Figure 9 we can observe the choices of right electrode locations for each patient, together with the corresponding PV loops. From these results we notice that there is a significant improvement of the stroke volume when the right electrode is located in the septal region halfway between the apex and the base. More in detail, from Table 7, where we report the best cases together with the standard one, we observe that for the non-fibrotic cases the improvements with respect to the pre-operative case in terms of SV, EF and SW almost double compared to the standard apical RE case. As regards the fibrotic cases, there is still an improvement of the three biomarkers compared to the RE case, even if milder.

On the other hand, for the non-fibrotic cases, $dP/dt|_{\max}$ does not appear to benefit from the upward movement of the right electrode along the septum, whereas slight improvements are noticed for the fibrotic cases.

4 Discussion

In this work we performed a computational study to assess the performance of CRT in terms of hemodynamic indices in different scenarios obtained by virtually varying the electrodes locations and their phase shift. To do this we carried out EM numerical simulations in three non-fibrotic and three fibrotic patients, suitably calibrated

Patient	Location	$dP/dt\|_{\mathbf{max}}$ [mmHg s^{-1}]	SV [ml]	EF [%]	SW [mmHg ml]
P2	*Pre-operative*	$2,252$	76	15.1	$6,300$
	RE	$+7.4\%$	$+11.8\%$	$+1.8$	$+19.4\%$
	RE 3	$+3.5\%$	$+19.7\%$	$+3.1$	$+33.4\%$
P3	*Pre-operative*	$3,119$	112	31.9	$11,600$
	RE	$+13.0\%$	$+8.0\%$	$+2.6$	$+14.8\%$
	RE 3	$+14.5\%$	$+12.5\%$	$+4.2$	$+22.3\%$
P4	*Pre-operative*	$2,278$	73	24.5	$6,800$
	RE	$+6.5\%$	$+7.3\%$	$+1.8$	$+10.8\%$
	RE 2	$+7.9\%$	$+12.2\%$	$+3.0$	$+19.3\%$
P6	*Pre-operative*	$2,186$	82	25.9	$7,000$
	RE	$+3.7\%$	$+11.8\%$	$+3.0$	$+16.9\%$
	RE 3	$+7.9\%$	$+12.5\%$	$+3.2$	$+19.3\%$
P8	*Pre-operative*	$2,731$	71	33.2	$6,700$
	RE	-7.5%	-1.4%	-0.3	-1.6%
	RE 2	-5.1%	$+8.5\%$	$+2.6$	$+11.3\%$
P11	*Pre-operative*	$2,460$	58	25.0	$4,900$
	RE	$+0.7\%$	$+10.3\%$	$+2.6$	$+15.6\%$
	RE 2	$+2.6\%$	$+12.1\%$	$+3.1$	$+19.6\%$

Table 7: Biomarkers corresponding to *virtual* CRT configurations varying right lead position, with LEAS choice for the left one and $VVD = 0$. *RE* position indicated the apical position used in the numerical experiments reported in Sections 3.3 and 3.4. See Figure 9 for the different locations of the right electrode. For CRT scenarios we indicate the percentage of variation of $dP/dt\|_{\max}$, *SV* and *SW* with respect to the pre-operative case, whereas for *EF* we indicate the absolute changes. P2, P3, P4: non-fibrotic cases; P6, P8, P11: fibrotic cases.

by means of EAMS and mechanical data, and compared some hemodynamic outputs of clinical interest. Our computational model incorporates an ionic model and a force generation model that are able to faithfully capture the frequency-dependent effects on the active force generation process, thus accounting for the different heart rates characterizing each patient.

This work featured some novelties in the framework of computational CRT studies:

- The validation of the calibrated EM model against EAMS measures obtained in a scenario (right pacing) different from that used for the calibration (no stimulations);

- The use of the calibrated and validated EM model in the context of CRT optimization;

- The use of the reconstruction of epicardial veins to identify anatomically compatible locations of the left electrode;

- The analysis of the CRT performance when different locations of the right electrode are exploited.

The outcomes of the EM numerical simulations were evaluated by computing four clinically relevant hemodynamic quantities. The Stroke Volume (SV) and the Ejection Fraction (EF) were used as a preliminary and easily computable indices of the restored synchronicity, although it is known that they are indicators of chronic reverse remodeling after CRT [1, 6, 52] rather than measures of acute outcomes. As a further index, we proposed to use the Stroke Work (SW) to have a more complete description of the mechanical properties of the ventricle, since it accounts also for the pressure jump within the cardiac cycle. We also analyzed the maximum variation of pressure during a cardiac cycle, $dP/dt\|_{max}$, employed to evaluate the synchronization and contractility of the cardiac muscle. This index has been used in other computational studies, e.g. in [14, 53], and it has been shown to be significant also in the acute regime [54, 51], since its acute increase of about 10% or more predicts reverse remodeling [55].

As regards the positioning of the left electrode, the clinical practice considers epicardial veins as a natural way to place it, for example in a lateral or posterolateral tributary of the coronary sinus [56, 57, 58] or in anterolateral and posterolateral locations [59]. Some studies proposed to consider measures of activation, for example coming from EAMS, and to locate the left electrode in the site with latest electrical activation (Latest Electrically Activated Segment, LEAS) [54, 46]. Other studies highlighted that the best location is specific to each individual, so it does not always match the latest activated segment [60]. Our results showed that the LEAS is an effective choice

to position the left electrode for the non-fibrotic cases, in terms of significant improvements of the hemodynamic indices with respect to the pre-operative case. Notice that our LEAS always falls in lateral (P6, P8), antero-lateral (P2, P4), or in anterior (P11) position. Moreover, we showed how it is possible to identify other locations in the epicardial veins that could even slightly improve the performance of LEAS.

As regards the ventriculo-ventricular delay, our results showed that for the non-fibrotic cases the activation of the right electrode before (15 or 30 ms) the left one seems to improve the CRT performance. This is in contrast with the clinical experience, where the left electrode is usually activated first, to compensate the delay of activation of the corresponding region [61]. However, some work has contradicted this indication, showing that there is no effective agreed rule in this regard [62, 63]. The interpretation of our findings relies on the observation that in the physiological (non-CRT) case the region where the right electrode is usually placed is activated by the Purkinje network slightly earlier than the region activated by the left electrode. Thus, anticipating the right stimulus can maybe restore a more physiological condition, allowing the ventricle to twist properly.

One of the novelties of this work relies on exploring different possible locations of the right electrode along the septum. In the clinical practice, usually this is placed in the apical position. However, some clinical studies suggested that other locations could be explored, see for example [57, 64, 58], where the authors proposed to place the right electrode in the mid-septum or in outflow tract septum. Accordingly, we virtually moved it in other positions which are compatible with anchoring by screwing to the septum [64], to understand if the performance of CRT could improve. We found that in general the performance in terms of EF, SV and SW seems to improve by positioning the electrode a little higher, towards the base. Although very preliminary and far to provide specific indications, we believe that this new analysis could provide a new horizon of exploration for the improvement of CRT and deserves further investigations.

One of the critical issues related to the good functioning of the therapy is the presence of fibrosis. Some clinical studies revealed that the presence of fibrosis (e.g. midwall fibrosis) could be an independent factor in favoring CRT non-responders [65, 66, 67]. For example in [65] the authors showed that the non-responders mainly consist of patients with scar tissue in the region of the left lead or with wide scar tissue. Our results went in this direction, highlighting that the improvements of all biomarkers are in general less noticeable than in the non-fibrotic cases. See also [68], where the authors computationally found that pacing at the LV epicardial surface in proximity to scar increases the volume of high repolarization gradients, thus explaining the CRT-induced ventricular tachycardia in patients with ischemia. Again, further investigations will be mandatory, for example to find possible correlations between the fibrosis region and the placement of the electrodes.

Finally, we remark that all the results of this work were found under a main assumption: the calibrated *pre-operative* parameters are considered to remain the same just after the CRT. This means that the electrical and mechanical properties of the heart muscle and the blood resistances do not change immediately after the implantation, since the LV needs over six months to experience remodeling [6]. This allowed us to use the pre-operative calibrated electro-mechanical parameters also for the virtual CRT scenarios.

To conclude, in this paper, we have showcased the practical application of our developed methodology on some specific patients. Our intention was not to conduct extensive statistical analyses, given the relatively modest sample size. Instead, our focus was on presenting a proof-of-concept to highlight the potential of the proposed methodology. The proposed pipeline was particularly well-suited for systematic replication on a patient-specific basis, requiring relatively low computational costs. This methodology could serve as the foundation for a routine procedure aimed at optimizing CRT with consideration for individualized factors, including geometric, electrophysiological, and mechanical aspects, and their complex interplay.

Limitations and further developments

There are several limitations in this work, which are discussed in what follows.

- We did not consider in our simulations the atria. This means that we were not able to take into account possible preload changes due to different atrio-ventricular delays [69]. Thus, our results should be understood as obtained under the hypothesis of sinus-rhythm atrio-ventricular delay;

- Our electrical calibration was based on measures obtained by means of an Electro-Anatomical Mapping System. Not all CRT interventions are nowadays made exploiting this procedure to guide the insertion of the electrodes and limit the radiation exposure. However, in the last years performing EAMS-assisted CRT is becoming more and more frequent, as proved by the multicentric study [70];

- We did not consider the Purkinje system in our electro-mechanical model. This simplification could have a significant impact on the results, due, e.g., to possible re-entries from the left stimulation front [71, 72];

- Our pipeline, from MRI images and EAMS measures to the numerical results of the virtual CRT scenarios, passing through the electro-mechanical calibration, is nowadays not completely automatic. Some steps are still manual (ventricle segmentation, electrical calibration), whereas other are completely automatic (mechanical calibration, building of nested meshes, generation of epicardial veins). In the future, we plan to make our procedure completely automatic, so in principle one could insert it as a module of EAMS;

- Our model calibration and numerical experiments ignore the right ventricle. This may have some important consequences on the results, since the left contraction is influenced by the right one. However, in view of the comparison among virtual scenarios, where we were interested more in relative differences than in absolute values, we believe that the effect of this approximation could be acceptable in this first study.

Several further developments will be considered in future works to make our procedure more accurate, efficient, and able to provide more precise clinical information. The previous limitations naturally suggest some of them: the inclusion of left atrium, right ventricle, and Purkinje network, and the full automation of the computational pipeline. Moreover, we will need to study more cases and to provide, through statistical analyses, more precise indications on the stimulations regions and delays that could imporve CRT, possibly clustering the patients in accordance with their conditions (presence of fibrosis, blocks, etc.).

References

[1] William T Abraham et al. "Cardiac resynchronization in chronic heart failure". *The New England Journal of Medicine* 346 (2002), pages 1845–1853.

[2] Jonathan A. Kirk and David A. Kass. "Electromechanical Dyssynchrony and Resynchronization of the Failing Heart". *Circulation Research* 113 (2013), pages 765–776.

[3] Victoria Delgado and Jeroen J. Bax. "Is Assessment of Systolic Dyssynchrony for Cardiac Resynchronization Therapy Clinically Useful?" *Circulation* 123 (2011), pages 640–655.

[4] Victoria Delgado et al. "Relative Merits of Left Ventricular Dyssynchrony, Left Ventricular Lead Position, and Myocardial Scar to Predict Long-Term Survival of Ischemic Heart Failure Patients Undergoing Cardiac Resynchronization Therapy". *Circulation* 123 (2011), pages 70–78.

[5] Angela W. C. Lee et al. "Biophysical Modeling to Determine the Optimization of Left Ventricular Pacing Site and AV/VV Delays in the Acute and Chronic Phase of Cardiac Resynchronization Therapy". *Journal of Cardiovascular Electrophysiology* 28 (2017), pages 208–215.

[6] Martin G. St John Sutton et al. "Effect of Cardiac Resynchronization Therapy on Left Ventricular Size and Function in Chronic Heart Failure". *Circulation* 107 (2003), pages 1985–1990.

[7] Jatin Relan, Phani Chinchapatnam, Maxime Sermesant, Kawal Rhode, Matt Ginks, Hervé Delingette, C. Aldo Rinaldi, Reza Razavi, and Nicholas Ayache. "Coupled personalization of cardiac electrophysiology models for prediction of ischaemic ventricular tachycardia". *Biomechanics and Modeling in Mechanobiology* 1 (3 2011), pages 396–407.

[8] B. T. Chan, C. W. Ong, E. Lim, N. A. Abu Osman, A. Al Abed, N. H. Lovell, and S. Dokos. "Simulation of left ventricle flow dynamics with dilated cardiomyopathy during the filling phase". In: *2012 Annual International Conference of the IEEE Engineering in Medicine and Biology Society*. 2012.

[9] Roy C.P. Kerckhoffs, Andrew D. McCulloch, Jeffrey H. Omens, and Lawrence J. Mulligan. "Effects of biventricular pacing and scar size in a computational model of the failing heart with left bundle branch block". *Medical Image Analysis* 13 (2009), pages 362–369.

[10] Jazmin Aguado-Sierra et al. "Patient-specific modeling of dyssynchronous heart failure: A case study". *Progress in Biophysics and Molecular Biology* 107 (2011), pages 147–155.

[11] A. Quarteroni, A. Manzoni, and C. Vergara. "The cardiovascular system: Mathematical modelling, numerical algorithms and clinical applications". *Acta Numerica* 26 (2017), pages 365–590.

[12] Angela WC Lee, Caroline Mendonca Costa, Marina Strocchi, Christopher A Rinaldi, and Steven A Niederer. "Computational modeling for cardiac resynchronization therapy". *Journal of cardiovascular translational research* 11 (2018), pages 92–108.

[13] Roy C. P. Kerckhoffs, Owen P. Faris, Peter H. M. Bovendeerd, Frits W. Prinzen, Karel Smits, Elliot R. McVeigh, and Theo Arts. "Timing of Depolarization and Contraction in the Paced Canine Left Ventricle: Model and Experiment". *Journal of Cardiovascular Electrophysiology* 14 (2003), S188–S195.

[14] M. Sermesant et al. "Patient-specific electromechanical models of the heart for the prediction of pacing acute effects in CRT: A preliminary clinical validation". *Medical Image Analysis* 16 (2012), pages 201–215.

[15] Eoin R. Hyde et al. "Beneficial Effect on Cardiac Resynchronization From Left Ventricular Endocardial Pacing Is Mediated by Early Access to High Conduction Velocity Tissue". *Circulation: Arrhythmia and Electrophysiology* 8 (2015), pages 1164–1172.

[16] Elham Kayvanpour et al. "Towards Personalized Cardiology: Multi-Scale Modeling of the Failing Heart". *PLOS ONE* 10 (7 2015), pages 1–18.

[17] Andrew Crozier et al. "The relative role of patient physiology and device optimisation in cardiac resynchronisation therapy: A computational modelling study". *Journal of Molecular and Cellular Cardiology* 96 (2016), pages 93–100.

[18] Caroline Mendonca Costa et al. "Left ventricular endocardial pacing is less arrhythmogenic than conventional epicardial pacing when pacing in proximity to scar". *Heart Rhythm* 17 (8 2020), pages 1262–1270.

[19] Matthias Reumann, Dima Farina, Raz Miri, Stephan Lurz, Brigitte Osswald, and Olaf Dössel. "Computer model for the optimization of AV and VV delay in cardiac resynchronization therapy". *Medical and Biological Engineering and Computing* 45 (2007), pages 845–854.

[20] Christopher T. Villongco, David E. Krummen, Jeffrey H. Omens, and Andrew D. McCulloch. "Non-invasive, model-based measures of ventricular electrical dyssynchrony for predicting CRToutcomes". *Europace* 18 (2016), pages iv104–iv112.

[21] Marieke Pluijmert, Peter HM Bovendeerd, Joost Lumens, Kevin Vernooy, Frits W Prinzen, and Tammo Delhaas. "New insights from a computational model on the relation between pacing site and CRT response". *EP Europace* 18 (2016), pages iv94–iv103.

[22] Akihiro Isotani, Kazunori Yoneda, Takashi Iwamura, Masahiro Watanabe, Jun ichi Okada, Takumi Washio, Seiryo Sugiura, Toshiaki Hisada, and Kenji Ando. "Patient-specific heart simulation can identify non-responders to cardiac resynchronization therapy". *Heart and Vessels* 35 (8 2020), pages 1135–1147.

[23] Lei Fan, Jenny S. Choy, Farshad Raissi, Ghassan S. Kassab, and Lik Chuan Lee. "Optimization of cardiac resynchronization therapy based on a cardiac electromechanics-perfusion computational model". *Computers in Biology and Medicine* 141 (2022), page 105050. ISSN: 0010-4825.

[24] Simone Stella, Francesco Regazzoni, Christian Vergara, Luca Dedé, and Alfio Quarteroni. "A fast cardiac electromechanics model coupling the Eikonal and the nonlinear mechanics equations". *Mathematical Models and Methods in Applied Sciences* 32 (2022), pages 1531–1556.

[25] Simone Stella, Christian Vergara, Massimiliano Maines, Domenico Catanzariti, Pasquale Claudio Africa, Cristina Demattè, Maurizio Centonze, Fabio Nobile, Maurizio Del Greco, and Alfio Quarteroni. "Integration of activation maps of epicardial veins in computational cardiac electrophysiology". *Computers in Biology and Medicine* 127 (2020), page 104047.

[26] Christian Vergara, Simone Stella, Massimiliano Maines, Pasquale Africa, Domenico Catanzariti, Cristina Demattè, Maurizio Centonze, Fabio Nobile, Alfio Quarteroni, and Maurizio Del Greco. "Computational electrophysiology of the coronary sinus branches based on electro-anatomical mapping for the prediction of the latest activated region". *Medical and Biological Engineering and Computing* 60 (2022), pages 1–13.

[27] Aurel Neic, Fernando O Campos, Anton J Prassl, Steven A Niederer, Martin J Bishop, Edward J Vigmond, and Gernot Plank. "Efficient computation of electrograms and ECGs in human whole heart simulations using a reaction-eikonal model". *Journal of computational physics* 346 (2017), pages 191–211.

[28] Francesco Zanon et al. "Multipoint pacing by a left ventricular quadripolar lead improves the acute hemodynamic response to CRT compared with conventional biventricular pacing at any site". *Heart Rhythm Society* 12 (2015), pages 975–981.

[29] Charlotte Eitel, Gerhard Hindricks, Nikolaos Dagres, Philipp Sommer, and Christopher Piorkowski. "EnSite Velocity™ cardiac mapping system: a new platform for 3D mapping of cardiac arrhythmias". *Expert Review of Medical Devices* 7 (2010), pages 185–192.

[30] Alejandro F Frangi, Wiro J Niessen, Koen L Vincken, and Max A Viergever. "Multiscale vessel enhancement filtering". In: *Medical Image Computing and Computer-Assisted Intervention—MICCAI'98: First International Conference Cambridge, MA, USA, October 11–13, 1998 Proceedings 1*. Springer. 1998, pages 130–137.

[31] Luca Antiga, Marina Piccinelli, Lorenzo Botti, Bogdan Ene-Iordache, Andrea Remuzzi, and David A Steinman. "An image-based modeling framework for patient-specific computational hemodynamics". *Medical & biological engineering & computing* 46 (2008), pages 1097–1112.

[32] Piero Colli Franzone, Luca Franco Pavarino, and Simone Scacchi. *Mathematical Cardiac Electrophysiology*. Springer Cham, 2014.

[33] Jakub Tomek et al. "Development, calibration, and validation of a novel human ventricular myocyte model in health, disease, and drug block". *eLife* 8 (2019). Edited by José D Faraldo-Gómez, Naama Barkai, Thomas Hund, and Molly Maleckar, e48890. ISSN: 2050-084X.

[34] Francesco Regazzoni, Luca Dedè, and Alfio Quarteroni. "Biophysically detailed mathematical models of multiscale cardiac active mechanics". *PLOS Computational Biology* 16 (2020), pages 1–42.

[35] Taras P Usyk, Ian J LeGrice, and Andrew D McCulloch. "Computational model of three-dimensional cardiac electromechanics". *Computing and Visualization in Science* 4 (2002), pages 249–257.

[36] Martyn P. Nash and Alexander V. Panfilov. "Electromechanical model of excitable tissue to study reentrant cardiac arrhythmias". *Progress in Biophysics and Molecular Biology* 85 (2-3 2004), pages 501–522.

[37] Nico Westerhof, Jan-Willem Lankhaar, and Berend E. Westerhof. "The arterial Windkessel". *Medical and Biological Engineering and Computing* 47 (2 2009), pages 131–141.

[38] Alfio Quarteroni, Alessandro Veneziani, and Christian Vergara. "Geometric multiscale modeling of the cardiovascular system, between theory and practice". *Computer Methods in Applied Mechanics and Engineering* 302 (2016), pages 193–252.

[39] Martin R. Pfaller, Julia M. Hörmann, Martin Weigl, Andreas Nagler, Radomír Chabiniok, Cristóbal Bertoglio, and Wolfgang A. Wall. "The importance of the pericardium for cardiac biomechanics: from physiology to computational modeling". *Biomechanics and Modeling in Mechanobiology* 18 (2018), pages 503–529.

[40] Jason D Bayer, Robert C Blake, Gernot Plank, and Natalia A Trayanova. "A novel rule-based algorithm for assigning myocardial fiber orientation to computational heart models". *Annals of biomedical engineering* 40 (2012), pages 2243–2254.

[41] Roberto Piersanti, Pasquale C Africa, Marco Fedele, Christian Vergara, Luca Dedè, Antonio F Corno, and Alfio Quarteroni. "Modeling cardiac muscle fibers in ventricular and atrial electrophysiology simulations". *Computer Methods in Applied Mechanics and Engineering* 373 (2021), page 113468.

[42] Pasquale Claudio Africa. "lifex: A flexible, high performance library for the numerical solution of complex finite element problems". *SoftwareX* 20 (2022), page 101252.

[43] Pasquale Claudio Africa, Roberto Piersanti, Francesco Regazzoni, Michele Bucelli, Matteo Salvador, Marco Fedele, Stefano Pagani, Luca Dede', and Alfio Quarteroni. "lifex-ep: a robust and efficient software for cardiac electrophysiology simulations". *BMC bioinformatics* 24 (2023), page 389.

[44] F. Regazzoni and A. Quarteroni. "Accelerating the convergence to a limit cycle in 3D cardiac electromechanical simulations through a data-driven 0D emulator". *Computers in Biology and Medicine* 135 (2021), page 104641. ISSN: 0010-4825.

[45] Leeor M Jaffe and Daniel P Morin. "Cardiac resynchronization therapy: history, present status, and future directions". *Ochsner Journal* 14 (2014), pages 596–607.

[46] Maurizio Del Greco, Alessandro Zorzi, Irene Di Matteo, Anna Cima, Massimiliano Maines, Carlo Angheben, and Domenico Catanzariti. "Coronary sinus activation patterns in patients with and without left bundle branch block undergoing electroanatomic mapping system–guided cardiac resynchronization therapy device implantation". *Heart Rhythm* 14 (2017), pages 225–233.

[47] Angelo Auricchio, Jiang Ding, Julio C Spinelli, Andrew P Kramer, Rodney W Salo, Walter Hoersch, Bruce H KenKnight, Helmut U Klein, and PATH-CHF Study Group 1. "Cardiac resynchronization therapy restores optimal atrioventricular mechanical timing in heart failure patients with ventricular conduction delay". *Journal of the American College of Cardiology* 39 (2002), pages 1163–1169.

[48] Bernard Thibault et al. "Acute haemodynamic comparison of multisite and biventricular pacing with a quadripolar left ventricular lead". *Europace* 15 (2012), pages 984–991.

[49] Alwin Zweerink, Odette AE Salden, Wouter M van Everdingen, Gerben J de Roest, Peter M van de Ven, Maarten J Cramer, Pieter A Doevendans, Albert C van Rossum, Kevin Vernooy, Frits W Prinzen, et al. "Hemodynamic optimization in cardiac resynchronization therapy: should we aim for dP/dtmax or stroke work?" *JACC: Clinical Electrophysiology* 5 (2019), pages 1013–1025.

[50] D.A. Kass, W.L. Maughan, Zhong Mao Guo, A. Kono, K. Sunagawa, and K. Sagawa. "Comparative influence of load versus inotropic states on indexes of ventricular contractility: Experimental and theoretical analysis based on pressure-volume relationships". *Circulation* 76 (1987). Cited by: 432, pages 1422–1436.

[51] David D Spragg, Jun Dong, Barry J Fetics, Robert Helm, Joseph E Marine, Alan Cheng, Charles A Henrikson, David A Kass, and Ronald D Berger. "Optimal left ventricular endocardial pacing sites for cardiac resynchronization therapy in patients with ischemic cardiomyopathy". *Journal of the American College of Cardiology* 56 (2010), pages 774–781.

[52] Paul Steendijk, Sven A. Tulner, Jeroen J. Bax, Pranobe V. Oemrawsingh, Gabe B. Bleeker, Lieselot van Erven, Hein Putter, Harriette F. Verwey and Ernst E. van der Wall, and Martin J. Schalij. "Hemodynamic Effects of Long-Term Cardiac Resynchronization Therapy". *Circulation* 113 (2006), pages 1295–1304.

[53] Gaëtan Desrues. "Personalised 3D electromechanical models of the heart for cardiac resynchronisation therapy planning in heart failure patients". PhD thesis. Université Côte d'Azur, 2023.

[54] Jagmeet P Singh, Dali Fan, E Kevin Heist, Chrisfouad R Alabiad, Cynthia Taub, Vivek Reddy, Moussa Mansour, Michael H Picard, Jeremy N Ruskin, and Theofanie Mela. "Left ventricular lead electrical delay predicts response to cardiac resynchronization therapy". *Heart Rhythm* 3 (2006), pages 1285–1292.

[55] Simon G Duckett, Matthew Ginks, Anoop K Shetty, Julian Bostock, Jaswinder S Gill, Shoaib Hamid, Stam Kapetanakis, Eliane Cunliffe, Reza Razavi, Gerry Carr-White, et al. "Invasive acute hemodynamic response to guide left ventricular lead implantation predicts chronic remodeling in patients undergoing cardiac resynchronization therapy". *Journal of the American College of Cardiology* 58 (2011), pages 1128–1136.

[56] Ole-A Breithardt, Christoph Stellbrink, Lieven Herbots, Piet Claus, Anil M Sinha, Bart Bijnens, Peter Hanrath, and George R Sutherland. "Cardiac resynchronization therapy can reverse abnormal myocardial strain distribution in patients with heart failure and left bundle branch block". *Journal of the American College of Cardiology* 42 (2003), pages 486–494.

[57] Caroline Vaillant, Raphaël P Martins, Erwan Donal, Christophe Leclercq, Christophe Thébault, Nathalie Behar, Philippe Mabo, and Jean-Claude Daubert. "Resolution of left bundle branch block–induced cardiomyopathy by cardiac resynchronization therapy". *Journal of the American College of Cardiology* 61 (2013), pages 1089–1095.

[58] Yao Wang, Haojie Zhu, Xiaofeng Hou, Zhao Wang, Fengwei Zou, Zhiyong Qian, Yongyue Wei, Xiang Wang, Longyao Zhang, Xiaofei Li, et al. "Randomized trial of left bundle branch vs biventricular pacing for cardiac resynchronization therapy". *Journal of the American College of Cardiology* 80 (2022), pages 1205–1216.

[59] Ying-Xue Dong, Brian D Powell, Samuel J Asirvatham, Paul A Friedman, Robert F Rea, Tracy L Webster, Kelly L Brooke, David O Hodge, Heather J Wiste, Yan-Zong Yang, et al. "Left ventricular lead position for cardiac resynchronization: a comprehensive cinegraphic, echocardiographic, clinical, and survival analysis". *Europace* 14 (2012), pages 1139–1147.

[60] Nicolas Derval, Paul Steendijk, Lorne J Gula, Antoine Deplagne, Julien Laborderie, Frederic Sacher, Sebastien Knecht, Matthew Wright, Isabelle Nault, Sylvain Ploux, et al. "Optimizing hemodynamics in heart failure patients by systematic screening of left ventricular pacing sites: the lateral left ventricular wall and the coronary sinus are rarely the best sites". *Journal of the American College of Cardiology* 55 (2010), pages 566–575.

[61] Henryk Dreger, Guido Antonow, Sebastian Spethmann, Hansjürgen Bondke, Gert Baumann, and Christoph Melzer. "Dyssynchrony parameter-guided interventricular delay programming". *Europace* 14 (2012), pages 696–702.

[62] Maria Cristina Porciani, Cristina Dondina, Roberto Macioce, Gabriele Demarchi, Paolo Pieragnoli, Nicola Musilli, Andrea Colella, Giuseppe Ricciardi, Antonio Michelucci, and Luigi Padeletti. "Echocardiographic examination of atrioventricular and interventricular delay optimization in cardiac resynchronization therapy". *The American journal of cardiology* 95 (2005), pages 1108–1110.

[63] Giuseppe Boriani, Mauro Biffi, Cord Paul Müller, KARL-HEINZ SEIDL, Rainer Grove, Jürgen Vogt, Wilfried Danschel, Andreas Schuchert, JEAN-CLAUDE DEHARO, Thorsten Becker, et al. "A prospective randomized evaluation of VV delay optimization in CRT-D recipients: Echocardiographic observations from the RHYTHM II ICD study". *Pacing and Clinical Electrophysiology* 32 (2009), S120–S125.

[64] Sarah A Worsnick, Parikshit S Sharma, and Pugazhendhi Vijayaraman. "Right ventricular septal pacing: a paradigm shift". *The Journal of Innovations in Cardiac Rhythm Management* 9 (2018), page 3137.

[65] Claudia Ypenburg, Martin J Schalij, Gabe B Bleeker, Paul Steendijk, Eric Boersma, Petra Dibbets-Schneider, Marcel PM Stokkel, Ernst E van der Wall, and Jeroen J Bax. "Impact of viability and scar tissue on response to cardiac resynchronization therapy in ischaemic heart failure patients". *European heart journal* 28 (2007), pages 33–41.

[66] Francisco Leyva, Robin J Taylor, Paul WX Foley, Fraz Umar, Lawrence J Mulligan, Kiran Patel, Berthold Stegemann, Tarek Haddad, Russell EA Smith, and Sanjay K Prasad. "Left ventricular midwall fibrosis as a predictor of mortality and morbidity after cardiac resynchronization therapy in patients with nonischemic cardiomyopathy". *Journal of the American College of Cardiology* 60 (2012), pages 1659–1667.

[67] Grégoire Massoullié, Vincent Sapin, Sylvain Ploux, Patrick Rossignol, Aurélien Mulliez, Frédéric Jean, Pierre-Yves Marie, Charles Merlin, Bruno Pereira, Marius Andronache, et al. "Low fibrosis biomarker levels predict cardiac resynchronization therapy response". *Scientific reports* 9 (2019), page 6103.

[68] Caroline Mendonca Costa, Aurel Neic, Eric Kerfoot, Bradley Porter, Benjamin Sieniewicz, Justin Gould, Baldeep Sidhu, Zhong Chen, Gernot Plank, Christopher A Rinaldi, et al. "Pacing in proximity to scar during cardiac resynchronization therapy increases local dispersion of repolarization and susceptibility to ventricular arrhythmogenesis". *Heart rhythm* 16 (2019), pages 1475–1483.

[69] Yuxuan Hu, Viatcheslav Gurev, Jason Constantino, and Natalia Trayanova. "Efficient preloading of the ventricles by a properly timed atrial contraction underlies stroke work improvement in the acute response to cardiac resynchronization therapy". *Heart Rhythm* 10 (2013), pages 1800–1806.

[70] Maurizio Del Greco, Massimiliano Maines, Massimiliano Marini, Andrea Colella, Massimo Zecchin, LAURA VITALI-SERDOZ, Alessandro Blandino, Lorella Barbonaglia, Giuseppe Allocca, Roberto Mureddu, et al. "Three-dimensional electroanatomic mapping system-enhanced cardiac resynchronization therapy device implantation: results from a multicenter registry". *Journal of Cardiovascular Electrophysiology* 28 (2017), pages 85–93.

[71] Mikel Landajuela, Christian Vergara, Antonello Gerbi, Luca Dedè, Luca Formaggia, and Alfio Quarteroni. "Numerical approximation of the electromechanical coupling in the left ventricle with insteclusion of the Purkinje network". *International journal for numerical methods in biomedical engineering* 34 (2018), e2984.

[72] Marina Strocchi, Karli Gillette, Aurel Neic, Mark K Elliott, Nadeev Wijesuriya, Vishal Mehta, Edward J Vigmond, Gernot Plank, Christopher A Rinaldi, and Steven A Niederer. "Effect of scar and His–Purkinje and myocardium conduction on response to conduction system pacing". *Journal of Cardiovascular Electrophysiology* (2023).
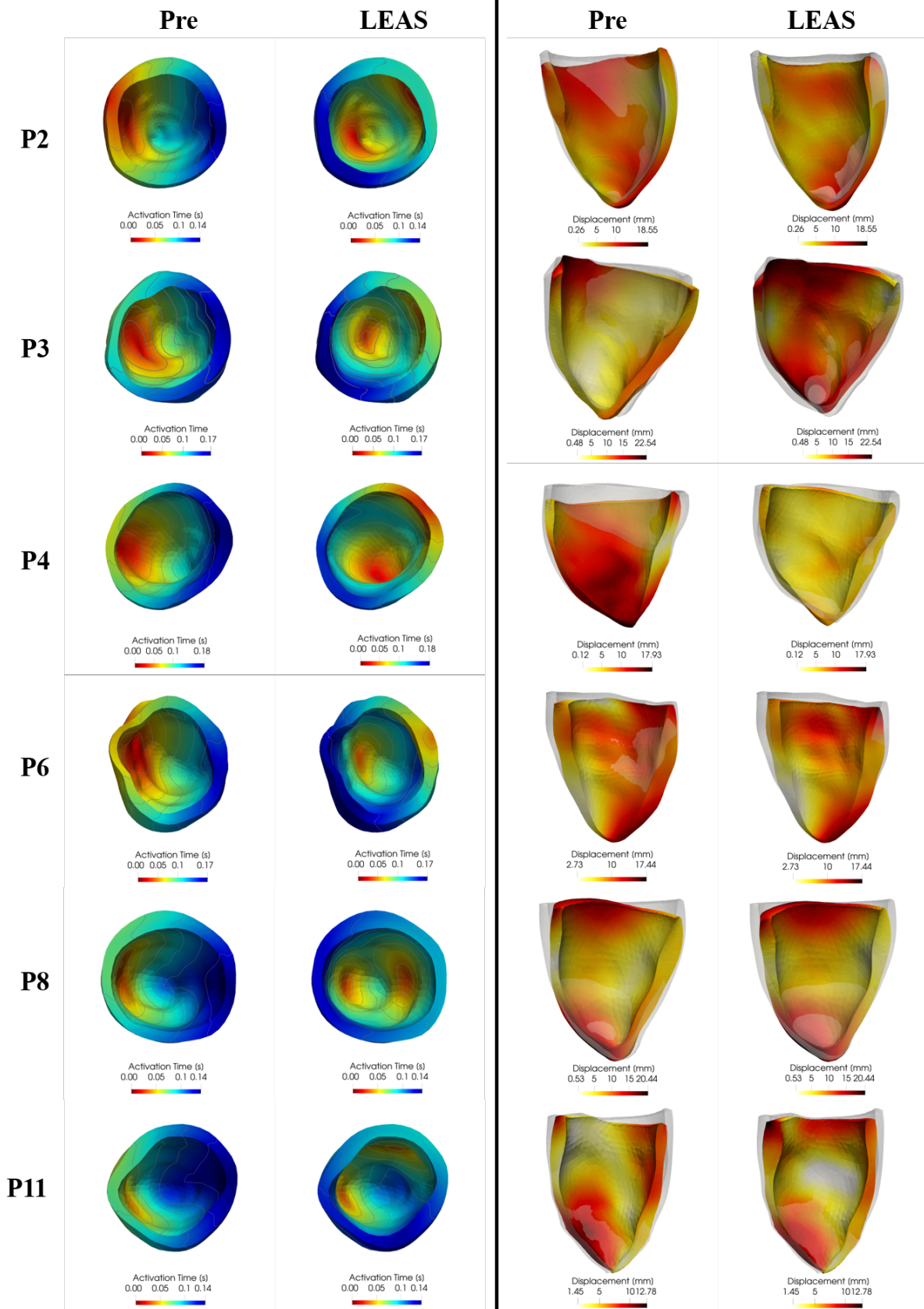
Figure 6: For each patient, comparison at a selected time of electrical activation times (left part) and mechanical contraction (right part) between the pre-operative scenario (left in each of the two parts of the figure) and the LEAS-based CRT virtual scenario (right).
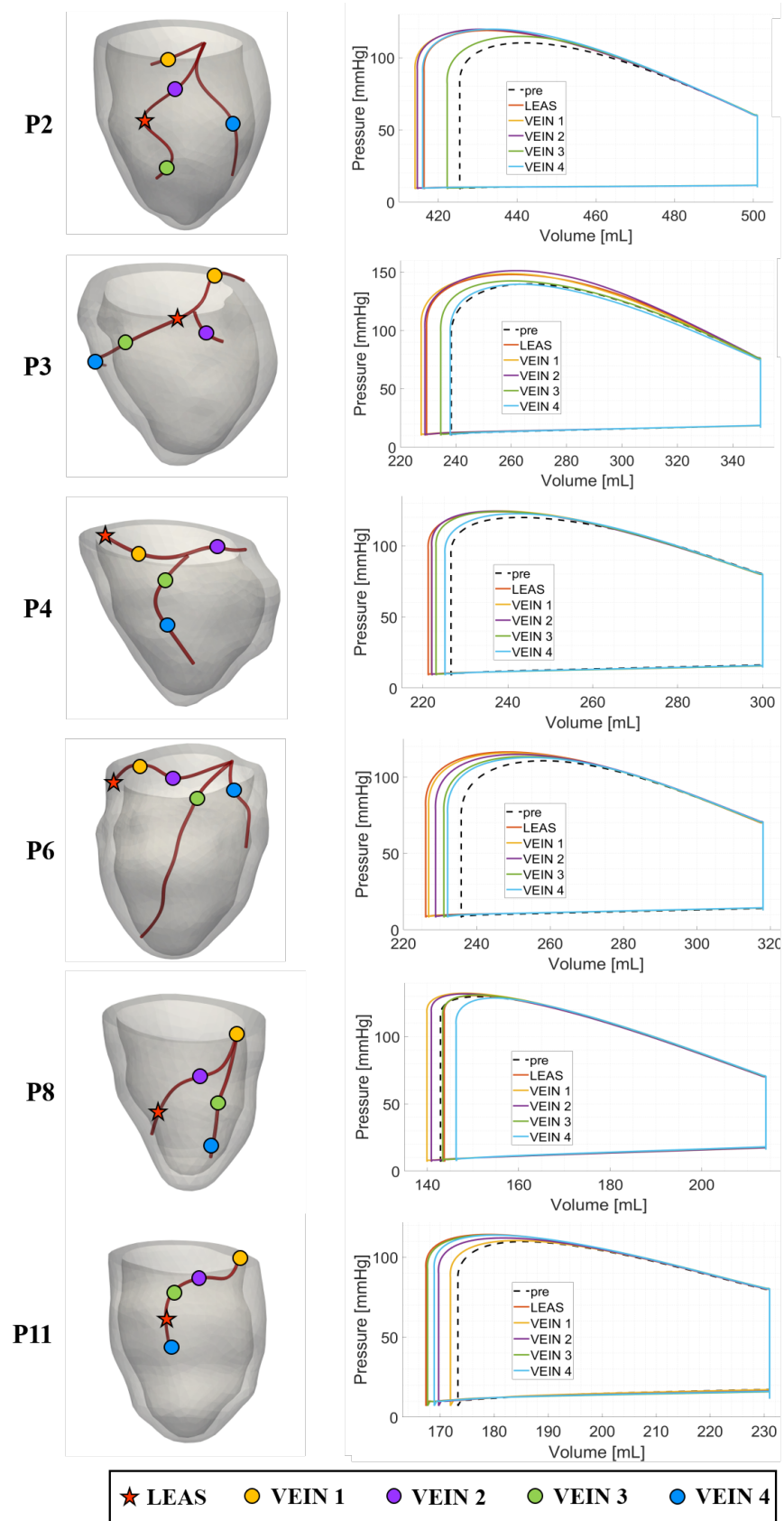
Figure 7: Representative choices of left electrode locations for virtual CRT simulations (left) and corresponding PV loops (right), overlapped to the pre-operative scenario.
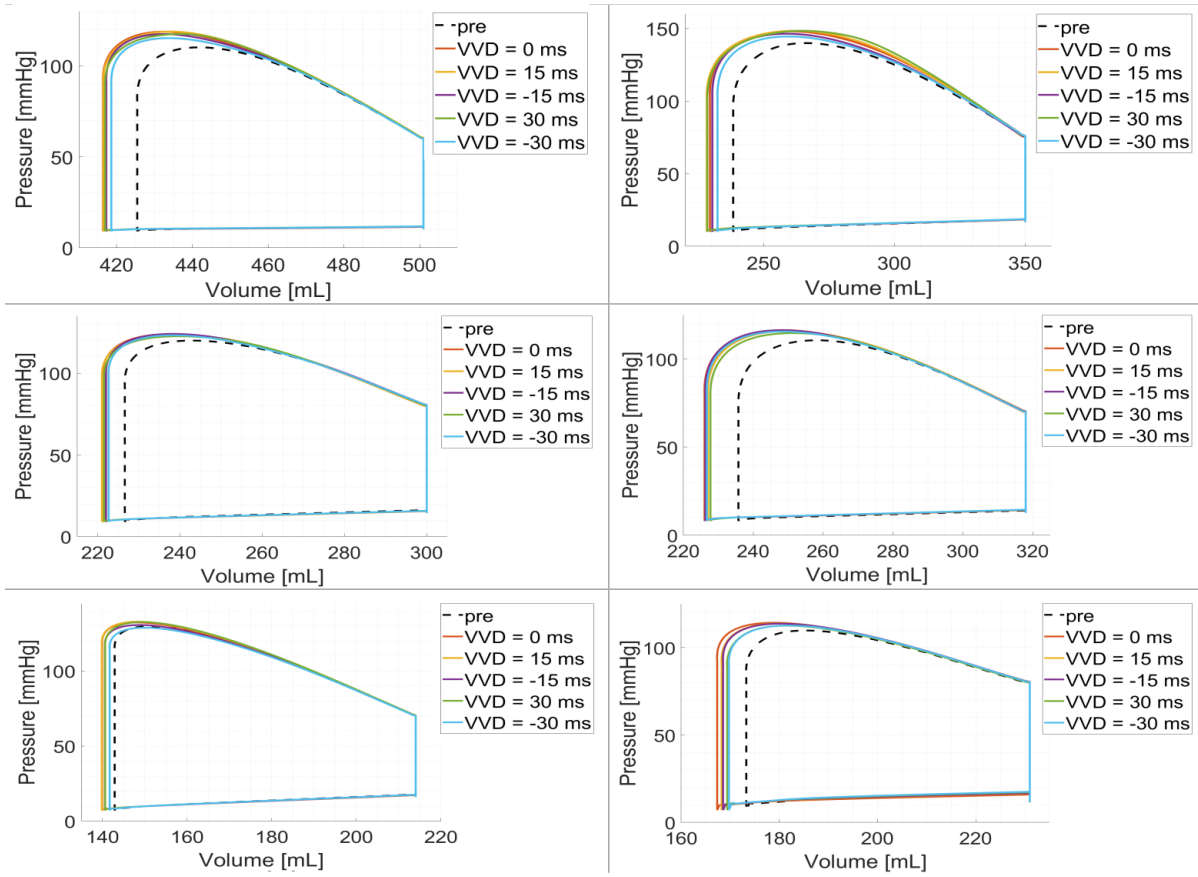
Figure 8: PV loops of the virtual CRT simulations at LEAS for five different choices of ventriculo-ventricular delay (VVD), overlapped to the pre-operative scenario.
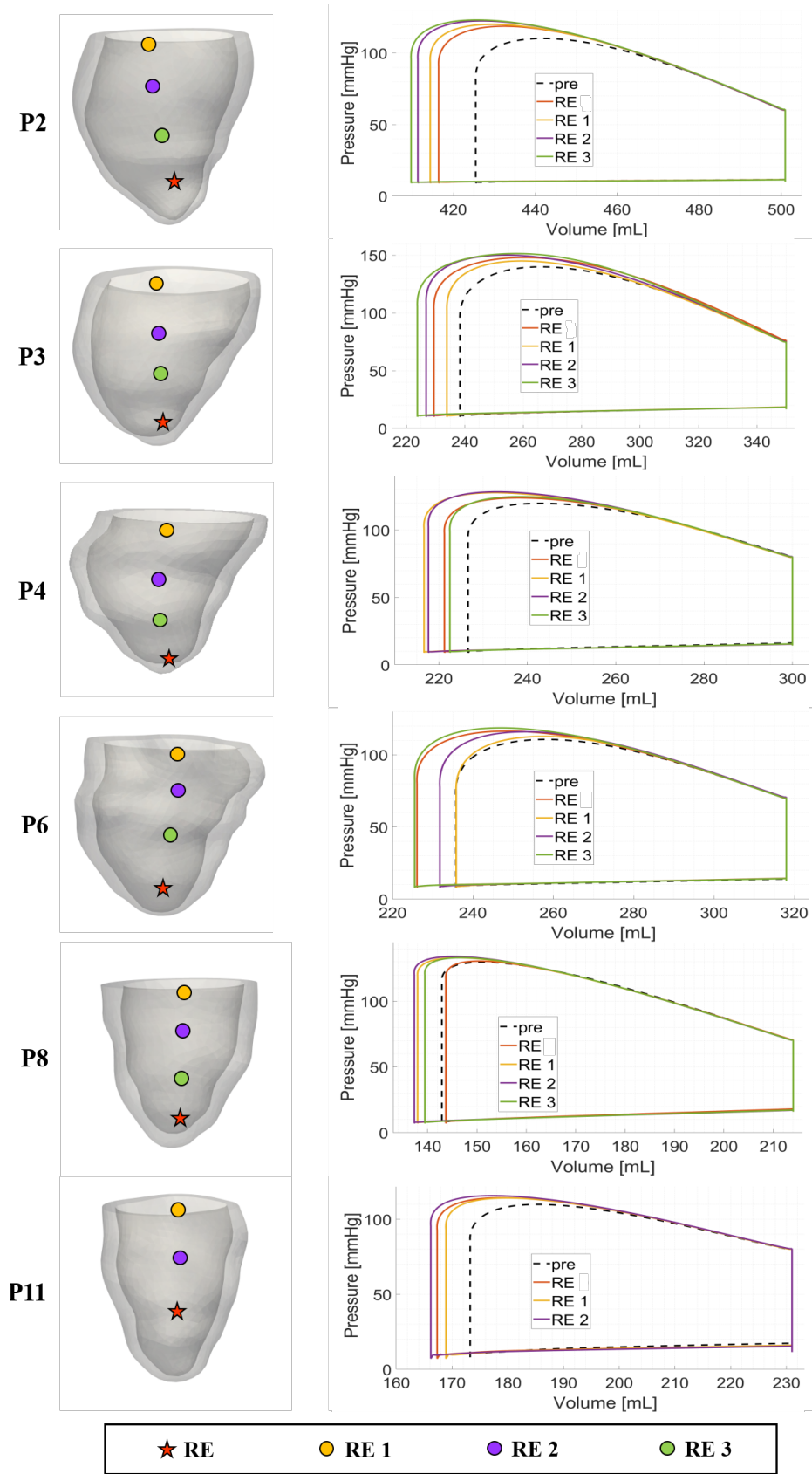
Figure 9: Choices of right electrode locations (RE) for virtual CRT simulations (left) and corresponding PV loops (right), overlapped to the pre-operative scenario. Left electrode placed at LEAS and no VV delay for all the cases.

MOX Technical Reports, last issues

Dipartimento di Matematica
Politecnico di Milano, Via Bonardi 9 - 20133 Milano (Italy)

09/2024   Leimer Saglio, C. B.: Pagani, S.; Corti, M.; Antonietti, P. F.
A high-order discontinuous Galerkin method for the numerical modeling of epileptic seizures

05/2024   Conti, P.; Gobat, G.; Fresca, S.; Manzoni, A.; Frangi, A.
*Reduced order modeling of parametrized systems through autoencoders and SINDy approach:
continuation of periodic solutions*

06/2024   Antonietti, P.F., Bonetti, S., Botti, M., Corti, M., Fumagalli, I., Mazzieri, I.
lymph: discontinuous poLYtopal methods for Multi-PHysics differential problems

04/2024   Torzoni, M.; Tezzele, M.; Mariani, S.; Manzoni, A.; Willcox, K.E.
A digital twin framework for civil engineering structures

03/2024   Ciaramella, G.; Gander, M.J.; Vanzan, T.
A gentle introduction to interpolation on the Grassmann manifold

Parolini, N.; Poiatti, A.; Vene', J.; Verani, M.
Structure-preserving neural networks in data-driven rheological models

02/2024   Parolini, N.; Poiatti, A.; Vene', J.; Verani, M.
Structure-preserving neural networks in data-driven rheological models

01/2024   Criseo, M.; Fumagalli, I.; Quarteroni, A.; Marianeschi, S. M.; Vergara, C.
*Computational haemodynamics for pulmonary valve replacement by means of a reduced
Fluid-Structure Interaction model*

109/2023   Clementi, L.; Arnone, E.; Santambrogio, M.D.; Franceschetti, S.; Panzica, F.; Sangalli, L.M.
Anatomically compliant modes of variations: new tools for brain connectivity

106/2023   Fontana, N.; Savaré, L.; Ieva, F.
*Integrating state-sequence analysis to uncover dynamic drug-utilization patterns to profile heart
failure patients*